Paper
Int'l J. of Aeronautical & Space Sci. 17(2), 157–166 (2016)
DOI: http://dx.doi.org/10.5139/IJASS.2016.17.2.157

IJASS
International Journal of Aeronautical and Space Sciences

Prediction of Aerodynamic Loads for NREL Phase VI Wind Turbine Blade in Yawed Condition

Ki-Wahn Ryu* and Seung-Hee Kang**

Department of Aerospace Engineering, Chonbuk National University, Jeonju 54896, Republic of Korea

Yun-Ho Seo***

Department of System Dynamics, Korea Institute of Machinery and Materials, Daejeon 34103, Republic of Korea

Wook-Ryun Lee****

Clean Power Generation Laboratory, KEPCO Research Institute, Daejeon 34056, Republic of Korea

Abstract

Aerodynamic loads for a horizontal axis wind turbine of the National Renewable Energy Laboratory (NREL) Phase VI rotor in yawed condition were predicted by using the blade element momentum theorem. The classical blade element momentum theorem was complemented by several aerodynamic corrections and models including the Pitt and Peters' yaw correction, Buhl's wake correction, Prandtl's tip loss model, Du and Selig's three-dimensional (3-D) stall delay model, etc. Changes of the aerodynamic loads according to the azimuth angle acting on the span-wise location of the NREL Phase VI blade were compared with the experimental data with various yaw angles and inflow speeds. The computational flow chart for the classical blade element momentum theorem was adequately modified to accurately calculate the combined functions of additional corrections and models stated above. A successive under-relaxation technique was developed and applied to prevent possible failure during the iteration process. Changes of the angle of attack according to the azimuth angle at the specified radial location of the blade were also obtained. The proposed numerical procedure was verified, and the predicted data of aerodynamic loads for the NREL Phase VI rotor bears an extremely close resemblance to those of the experimental data.

Key words: horizontal axis wind turbine, aerodynamic loads, NREL Phase VI rotor, blade element momentum theorem (BEMT)

1. Introduction

The total amount of power of the cumulative installations of offshore wind turbines in the world increased to 8,759 MW in 2014, and 91 % of all offshore wind turbines are located in European waters [1]. Although most substructures until now are mono-pile types, the suction bucket foundation has attracted the attention of many utility operators because its installation is faster and its cost is lower than those of conventional foundations. In particular the suction bucket foundation can innovatively reduce the noise impact on marine animals and the environment. Recently the suction bucket type was adopted as foundations for the meteorological mast for HeMosu-2 and the 2.5 GW class offshore wind farm project southwest of the Korean peninsula [2]. Basically, suction buckets are a foundation structure that allows very weak ocean floor soils to provide the necessary support of extremely heavy superstructure loads. In design stage engineers are particularly concerned for the safe operation of the wind turbine system while maintaining vertical alignment against the aerodynamic loads in an extreme condition. Therefore, the load analysis for the wind turbine system

* Professor, Corresponding author: kwryu@chonbuk.ac.kr
** Associate Professor
*** Senior Researcher
**** Senior Researcher

Received: March 22, 2016 Revised: June 7, 2016 Accepted: June 21, 2016

http://ijass.org pISSN: 2093-274x eISSN: 2093-2480

based on a design regulation such as IEC 61400 [3] becomes indispensable to overcome the excessive aerodynamic and hydrodynamic forces acting on the support structure. From the above point of view, both thrust and overturning moment for the large-scaled horizontal axis wind turbine (HAWT) installed at an offshore wind farm are very significant parameters in the design of the supporting structure of the wind turbine system.

Most comprehensive codes such as FAST [4] for the wind turbine system have utilized the blade element momentum theorem (BEMT) for aerodynamic loads analysis in complicated flow condition including flow direction and flow speed changes. The considerable advantage of the BEMT is fast evaluation of the aerodynamic performance, while using reliable airfoil data from wind tunnel experiments. Thus, it can effectively provide useful aerodynamic data for analysis of solid structures, system dynamics, and control purposes in the design stage. Since axisymmetric assumption of the classical BEMT [5-6] for a wind turbine system without yaw is inapplicable to a yawed wind turbine system, computing procedure should be modified based on appropriate aerodynamic theories. One of the main causes of the complicated flow condition is the yaw error of the wind turbine rotor. The computing procedure for the classical BEMT without yaw error consists of an inner iteration loop for convergence and an outer repetition loop for blade elements [7]. However, the modified BEMT for the yaw error case requires an additional outermost iteration for the varying azimuth angle of the blade, and more aerodynamic corrections and models should be complemented in the flow chart. Many research groups have developed modified BEMT programs, and have been engaged in the 'Blind Comparison' for a specified wind turbine to enhance the performance of their developed code. For a typical case, National Renewable Energy Laboratory (NREL) organized a 'Blind Comparison' for wind turbine research institutes in the fall of 2000. After carrying out the blind test they concluded that the main differences among the different design codes depend on the airfoil coefficients table used and on the correction models used for rotational effects [8, 9].

The main purpose of this study is to develop an aerodynamic analysis code for a horizontal axis wind turbine blade with yaw error based on the modified BEMT. The aerodynamic loads and inflow angles of the predicted data for the NREL Phase VI rotor in yawed condition will be compared with those of the experimental data to verify the developed program. Based on this validation, the developed program will be joined with other interdisciplinary research routines such as aeroelasticity, and dynamic control for a comprehensive code for the wind turbine system, which will be supervised by Korea Electric Power Research Institute.

2. Aerodynamic Models and Numerical Procedure

2.1 Classical Blade Element Momentum Theorem

Blade element momentum theorem (BEMT) has been widely used for shape design and performance analysis of wind turbine blades because of its fast calculation and reasonable results. In particular, it can offer various engineering data for structural and dynamic problems in the design stage of the wind turbine system, and has consequently been adopted in most of the comprehensive codes such as FAST, BLADED, and PHATAS. Basic assumptions for the blade element momentum theorem include steady, one-dimensional (1-D), axisymmetric, inviscid, incompressible, irrotational, and uniform. Blade element momentum theorem combines two existing theories: the blade element theory for a two-dimensional (2-D) blade section and the 1-D momentum theory around the rotor. The blade element theory divides the blade into several small elements, and obtains the thrust and torque from the experimental data of the airfoil at a given angle of attack. The thrust and torque can also be calculated using the 1-D momentum theory with axial and tangential induction factors. If the two equations from each theory for thrust are made equal, an expression for the axial induction factor a is obtained:

$$a = \frac{V-u}{V} = \left\{1 + \frac{4\sin^2\phi}{\sigma[c_l\cos\phi + c_d\sin\phi]}\right\}^{-1} \tag{1}$$

where V is the wind speed at far field, u is the wind speed for axial direction at the rotor plane, and ϕ denotes the flow angle. The local solidity σ and angle of attack α can be expressed as follows:

$$\sigma = \frac{Bc}{2\pi r} \tag{2}$$

$$\alpha = \phi - \theta \tag{3}$$

where θ is the twist angle at the radial location r of the blade. Similarly, if the two equations from blade element theory and blade momentum theory for torque are made equal, an expression for the tangential induction factor a' is obtained:

$$a' = \frac{w}{\Omega r} = \left\{-1 + \frac{4\sin\phi\cos\phi}{\sigma[c_l\sin\phi - c_d\cos\phi]}\right\}^{-1} \tag{4}$$

where w is the flow speed along the tangential direction at rotor plane, and Ω is the angular speed of the wind turbine

DOI: http://dx.doi.org/10.5139/IJASS.2016.17.2.157

rotor.

The trailing vortices generated from the blade tips induce an axial wind component opposite to the free stream direction and a tangential direction opposite to the rotating direction. Fig. 1 shows the velocity triangle reflecting the induced velocities for a section of the blade. From the definition of axial and tangential induction factors and the velocity triangle, the flow angle can be directly derived from Fig. 1 as follows:

$$\phi = \tan^{-1}\frac{V(1-a)}{\Omega r(1+a')} \tag{5}$$

Some corrections and modifications have been continuously applied to the original theorem to solve the complicated flow cases which oppose the basic assumptions on the classical BEMT. For example, while axisymmetric flow with no yaw error is one of the basic assumptions, most of the wind turbine rotors are operated in the yawed condition. In this case periodic change of the angle of attack at the specified radial position of the blade generates cyclic variations of loads and moments at the hub, low speed shaft, and support structures according to the azimuth angle of the blade. To solve these problems, the classical BEMT should be corrected to reflect the yaw angle effects. The following sections investigate compensation methods for the classical BEMT.

2.2 Corrections for Airfoil Data

The 2-D aerodynamic data of the airfoil from an experiment in operating the Reynolds number is the most important input for the aerodynamic performance prediction of a wind turbine blade; however, it requires a number of specific corrections to provide accurate results. Namely, the inappropriate use of the airfoil data without correction can lead to inaccurate results. Therefore, adopting specific corrections for the airfoil data based on the aerodynamic knowledge is essential to obtaining accurate results. Both the stall delay model and the polar extrapolation of airfoil data are typical corrections for the airfoil data.

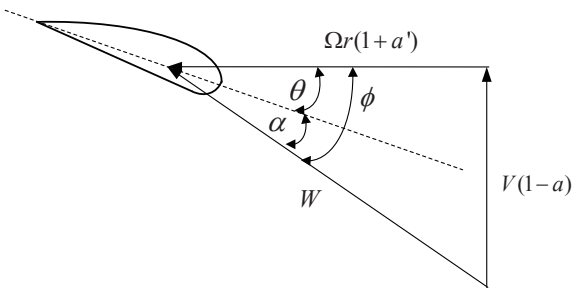

Fig. 1. Flow velocity diagram at an annulus in an HAWT rotor disc

When a blade is rotating on a hub axis, the fluid element passing the blade surface in the boundary layer tends to move in an outward radial direction due to the centrifugal force. This moving phenomenon generates an additional force towards the trailing edge of the airfoil by the Coriolis' effect; actually, Himmelskamp indicated that stall delay and lift enhancement occur for the rotating blade [10]. Du and Selig's 3-D stall delay model [11] is adopted in this current study.

The wind tunnel experiment of an airfoil in the entire range of angles of attack seems to be inefficient in terms of time and cost. Furthermore, the aerodynamic data of an airfoil in the strong stall state is very close to those of a flat plate, regardless of airfoil shapes. Thus, most of the angle of attack in the wind tunnel experiment is limited to the approximate range of -30° ~ +30°. The entire range of the airfoil data, however, is still necessary to predict the aerodynamic performance of the blade numerically without any iteration problems. To overcome this problem a number of polar extrapolations of the airfoil data in the limited range of the angle of attack have been proposed. Of these, the Viterna-Corrigan extrapolation of the airfoil data is adopted for this study [12].

2.3 Other Corrections

The physical mechanism for generating lift on the blade is the presence of high pressure on the windward surface and a low pressure on the leeward surface of the blade. The flow pattern due to this pressure imbalance near the wing tip tends to create rotational flow around the tip, and generates high strength of the trailing vortices. These tip vortices contain a large amount of translational and rotational kinetic energy. Since this energy of the vortices serves no useful power generation, the energy is essentially lost. The generated lift at the tip of the blade approaches zero; thus, the tip loss model should be adopted to compensate the deficiency in the classical BEMT. This study uses the Prandtl's tip loss model [5]. A tip loss factor F was introduced to correct the distribution of power along the blade span as follows:

$$F = f_R f_H \tag{6}$$

and

$$f_R = \frac{2}{\pi}\cos^{-1}(e^{-g_R}) \tag{7}$$

$$f_H = \frac{2}{\pi}\cos^{-1}(e^{-g_H}) \tag{8}$$

$$g_R = \frac{B}{2}\frac{R-r}{r\sin\phi} \tag{9}$$

$$g_H = \frac{B}{2}\frac{r - r_H}{r_H \sin\phi} \tag{10}$$

where B is the number of blades, R is the overall radius of the rotor, r is the local radius, and r_H is the hub radius. The corrected influence factors for Eqs. (1) and (4) can then be modified as follows:

$$a = \left\{1 + \frac{4F\sin^2\phi}{\sigma[c_l\cos\phi + c_d\sin\phi]}\right\}^{-1} \tag{11}$$

$$a' = \left\{-1 + \frac{4F\sin\phi\cos\phi}{\sigma[c_l\sin\phi - c_d\cos\phi]}\right\}^{-1} \tag{12}$$

The thrust coefficient as a function of the axial induction factor a derived from the Rankine-Froude actuator disc model shows a convex parabolic curve, of which the maximum thrust coefficient is 1.0 at a = 0.5. When the induction factor is greater than approximately 0.4, the wind turbine state reaches a turbulent wake state, and the basic assumption for the Rankine-Froude actuator disc model is no longer valid. Consequently, the relation between the thrust coefficient and axial induction factor shows very poor agreement for operation in a high induction state. Glauert, Wilson *et al.* [6] proposed empirical forms that fit with the measured data. Recently Buhl investigated the mismatch between the classical curve and the empirical curve, and derived of a new curve that accounts for the tip and hub losses and eliminates the numerical problems of the previous approaches [13]. He produced a quadratic expression that tangentially touches a curve from the classical momentum equation at a = 0.4 and proceeds through 2 at a = 1 as follows:

$$c_T = \frac{8}{9} + \left(4F - \frac{40}{9}\right)a + \left(\frac{50}{9} - 4F\right)a^2 \tag{13}$$

or

$$a = \frac{18F - 20 - 3\sqrt{c_T(50 - 36F) + 12F(3F - 4)}}{36F - 50} \tag{14}$$

The Glauert empirical relationship was determined for the overall thrust coefficient for a rotor. It is customary to assume that it applies equally to equivalent local thrust coefficients for each blade section. The thrust coefficient in Eq. (13) represents the local thrust coefficient, and it can be derived from the blade element theory as follows [14]:

$$c_T = \frac{dT}{\rho u^2 dA/2} = \frac{\sigma(1-a)^2[c_l\cos\phi + c_d\sin\phi]}{\sin^2\phi} \tag{15}$$

where dT denotes the local thrust on the blade element and dA=2$\pi$$rdr$ is the cross-sectional area of the annular element to be used in the blade element momentum model. If c_T is greater than 0.96F, Eq. (14) is applied to correct the axial induction factor [15]. In Fig. 2 the three expressions for the thrust coefficient are plotted for F = 1.

Generally, wind turbines have a yaw angle relative to the incoming wind direction during normal operation. In this case, the flow angle can be changed while considering the yaw angle:

$$\phi = \tan^{-1}\frac{u_z}{u_t} = \tan^{-1}\frac{V(1-a)\cos\gamma}{\Omega r(1+a') + V\sin\gamma\cos\psi} \tag{16}$$

where γ and ψ denote the yaw angle and azimuth angle of the blade, respectively. Thus, instead of Eq. (5), Eq. (16) should be used to calculate the flow angle for the yawed condition. Basically the classical blade element momentum theorem is obtained from the axisymmetric condition in which the rotating axis coincides exactly with the wind direction. Therefore the classical blade element momentum theorem should be corrected for the yawed condition. Glauert proposed a simple first harmonic non-uniform inflow model which generates an induced velocity field that increases longitudinally from the leading edge to the trailing edge of the rotor disc with the specified gradient [16]. Pitt and Peters [17] developed a complete dynamic inflow model for a forward flight helicopter rotor using the unsteady actuator disc theory. From the harmonic inflow model the axial induction becomes:

$$a = a\left(1 + \frac{15\pi}{32}\frac{r}{R}\tan\frac{\chi}{2}\cos\psi\right) \tag{17}$$

$$\chi = (0.6a + 1)\gamma \tag{18}$$

where χ represents the wake skew angle proposed by Burton *et al.* [18].

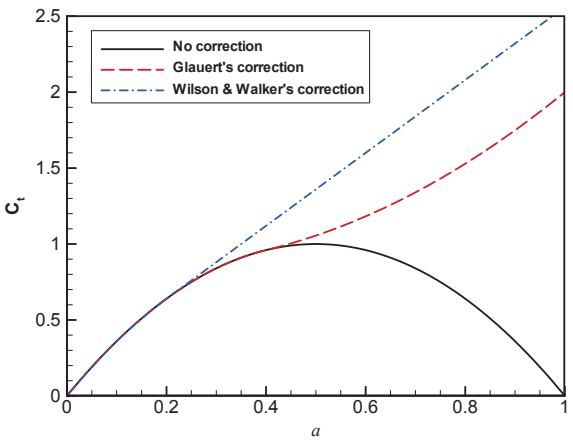

Fig. 2. Different expressions for the thrust coefficient versus the axial induction factor.

DOI: http://dx.doi.org/10.5139/IJASS.2016.17.2.157

2.4 Numerical Procedure

The numerical procedure is shown in Fig. 3, including the additional corrections to compensate for the classical BEMT for the yawed condition. It has three major loops: the inner-most iteration for flow angle at the specified blade element, the repetition for the blade element from hub to tip, and the outer-most repetition for the azimuth angle. During iterative calculation in the inner-most loop, an extrapolated aerodynamic table of the S809 airfoil is applied to extract the corresponding lift, drag, and moment coefficients at a given angle of attack. Occasionally, the iteration process failed due to an abrupt change of the predicted value. A successive under-relaxation technique is thus proposed and applied to prevent a possible failure during the iteration process as follows:

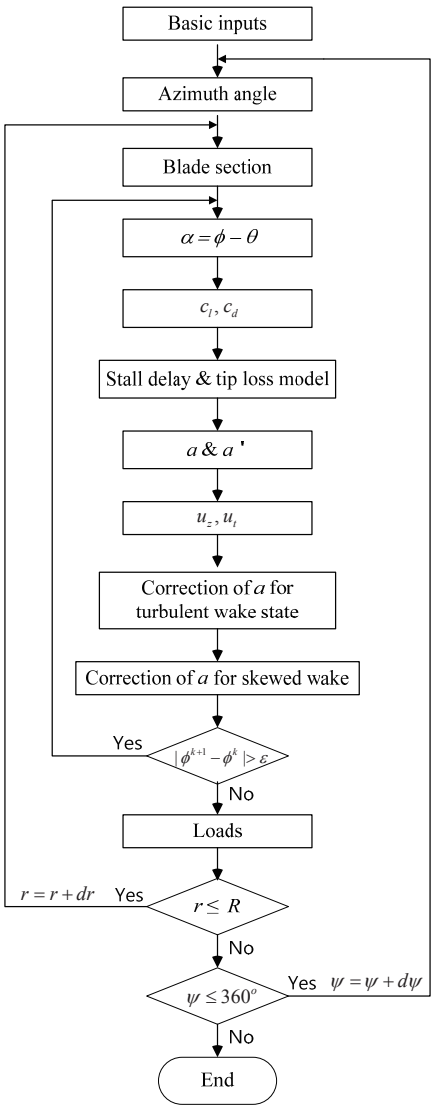

Fig. 3. Flow chart for yawed HAWT

$$\phi^{k+1} = \omega\tilde{\phi}^{k+1} + (1-\omega)\phi^k \tag{19}$$

where ϕ^{k+1} and ϕ^k represent the new and previous values of the inflow angle, respectively, ω is the relaxation factor, and $\tilde{\phi}^{k+1}$ denotes the newly calculated value to be corrected. In this study, ω = 0.1 is used with no divergence problem. The under-relaxation technique leads to stable convergence, although it has a weak point when increasing the computing time.

3. Results and Discussion

The NREL Phase VI rotor is a test model designed for unsteady aerodynamic experiments (UAE) [19]; it is two-bladed, twisted, and has a tapered shape with an S809 airfoil over the entire span. The model test was performed in the 24.4 m × 36.6 m wind tunnel of the NASA Ames research center, and pressure distributions were measured at r/R = 0.3, 0.47, 0.63, 0.8, and 0.95 radial positions. The measurements at 30° yaw were performed for tunnel speeds ranging between 5 m/s and 17 m/s. Measurements using the NASA-Ames wind tunnel are very suitable for validating large size yaw models. The S809 airfoil is a 21% thickness laminar-flow airfoil with a sharp trailing edge for the horizontal axis wind turbine. The wind tunnel data of the S809 airfoil, previously tested at the Ohio State University [20], will be used for aerodynamic performance analysis with a modified BEMT. Fig. 4 shows the S809 airfoil shape and distribution of drag, lift, and moment coefficients with respect to angles of attack at the Reynolds number of 1.5×10^6. The specifications and operating conditions for the NREL Phase VI rotor are summarized in Table 1. In this study, the predicted axial loads and inflow angles of attack for the NREL Phase VI rotor in 30° yawed condition will

Table 1. Operating condition of NREL Phase VI bade

Descriptions	Value
Number of blades	2
Rated power [kW]	19.8
Power regulation	Stall
Rotational speed [rpm]	71.63, synchronous 90, variable speed
Tilt angle	0
Rotor diameter [m]	10.058
Hub height [m]	12.192
Rotational direction (viewed from upward)	CCW
Cut-in wind speed [m/s]	5

be compared with measured data at two selected tunnel speeds of 10 m/s and 15 m/s.

The variation of angles of attack according to azimuth angle was investigated as shown in Fig. 5. The curves of the angle of attack at 4 radial positions of r/R = 0.47, 0.63, 0.80, and 0.95 for a wind speed of 10 m/s is periodically oscillated due to the yaw error. From the results we can determine two characteristics of the NREL Phase VI blade. Firstly, there is a larger angle of attack at the inboard portion of the blade than at the outboard portion. Usually, the angle of attack is a function of both flow and twist angles so that the inboard stall phenomenon can be adjusted. We can therefore conclude that the stall phenomenon will be initiated at the inboard rather than outboard region of the given NREL Phase VI blade.

Secondly, the yaw error changes the flow angle. The NREL Phase VI rotor was designed to rotate in the counter-clockwise direction. Clear definitions of the azimuth and yaw angles are a prerequisite for comparison of the predicted results with experiment data. The blade azimuth angle is defined as zero for the blade pointing down in the vertical position, i.e. the 6 o'clock position [19]. For positive yaw, the upwind side of the rotor plane can be defined between 0 and 180 degrees azimuth, where for negative yaw, this upwind side is between 180 and 360 degrees azimuth [19] as shown in Fig. 6, whilst NREL defines that the zero azimuth angle is at the 12 o'clock position and the yaw angle has the opposite sign to the present definition. For positive yaw, the blade is fully retreated at the 12 o'clock position, and advanced at the 6 o'clock position with respect to the in-plane wind component. This phenomenon yields sinusoidal variation of the angle of attack per revolution, and the flow angle from Eq. (16) will be maximized at the 12 o'clock position, and *vice versa*. Therefore, the angle of attack will be maximized at the 12 o'clock position. The predicted results for the angle of attack at r/R = 0.47, 0.63, 0.80, and 0.95 for a wind speed of 10 m/s clearly explain the case mentioned above as shown in Fig. 5.

The predicted normal forces using modified BEMT at the four radial positions of r/R = 0.47, 0.63, 0.80, and 0.95 for a wind speed of 10 m/s are compared with corresponding measured data as shown in Fig. 7. The normal force can be calculated from following equation:

$$F_n = \rho W^2 (c_l \cos\phi + c_d \sin\phi)/2, \quad [\text{Pa}] \tag{20}$$

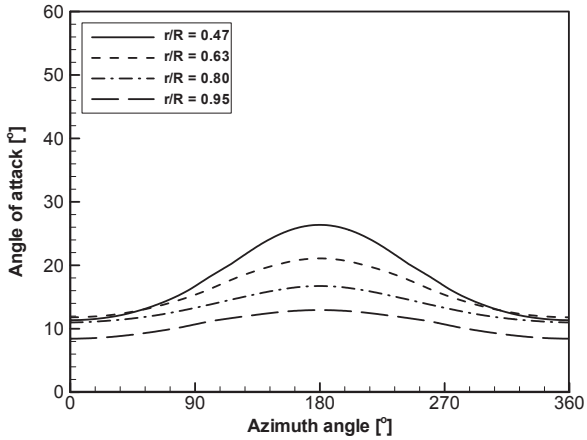

Fig. 5. Variation of angle of attack (V = 10 m/s, yaw angle = 30°)

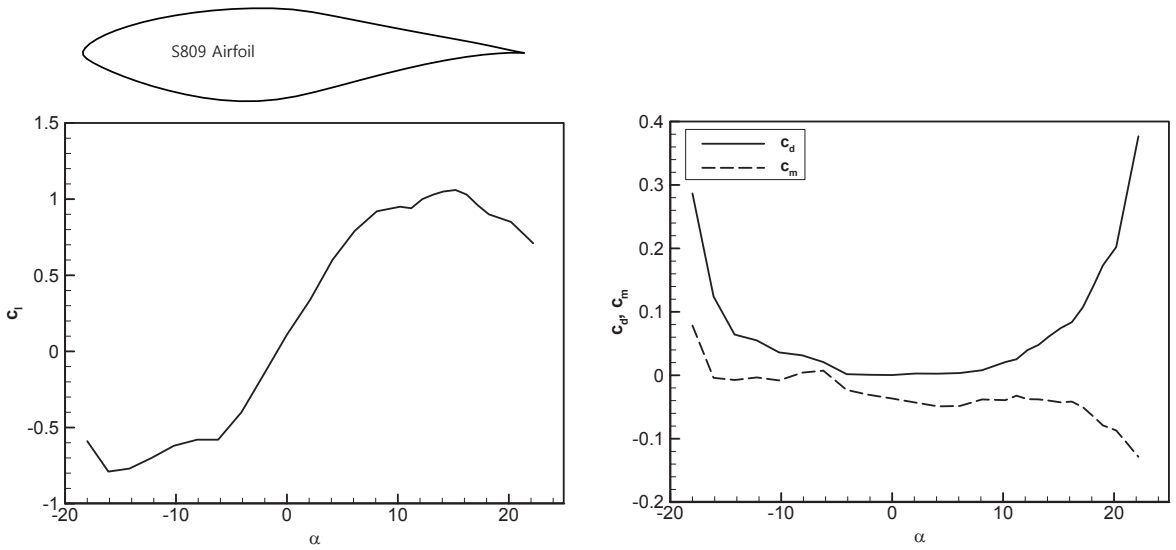

(a) Lift curve

(b) Drag and moment curves

Fig. 4. Aerodynamic data for S809 airfoil

DOI: http://dx.doi.org/10.5139/IJASS.2016.17.2.157

where W is the magnitude of relative velocity which is a vector sum of the axial velocity and the tangential velocity at the specified radial location on the disc plane. Except for the tip position at r/R = 0.95, the computed results based on the modified BEMT closely agree with the experimental data. All of the normal forces indicate minimum values at the

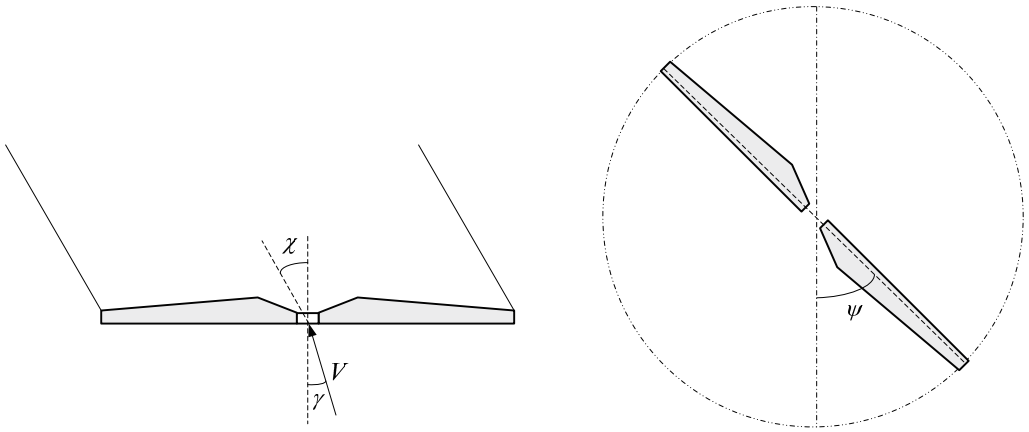

(a) Top view (b) Front view

Fig. 6. Yaw and wake skew angles

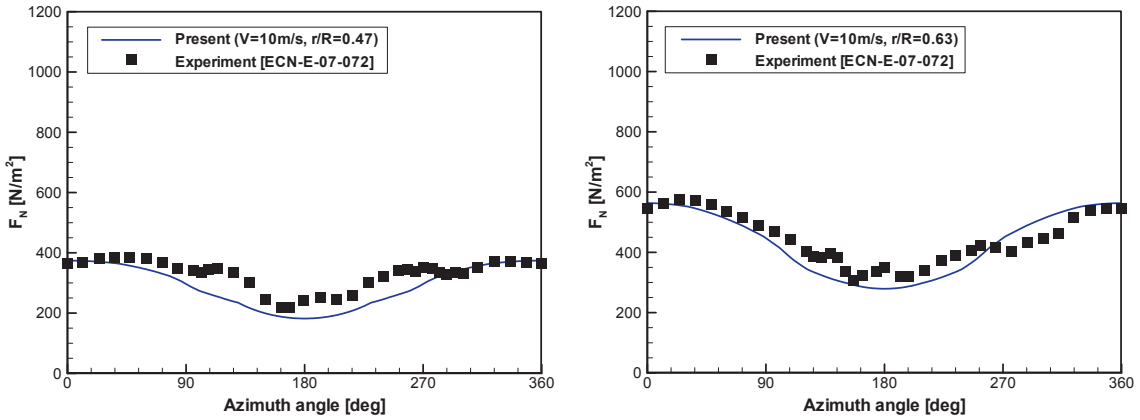

(a) r/R = 0.47

(b) r/R = 0.63

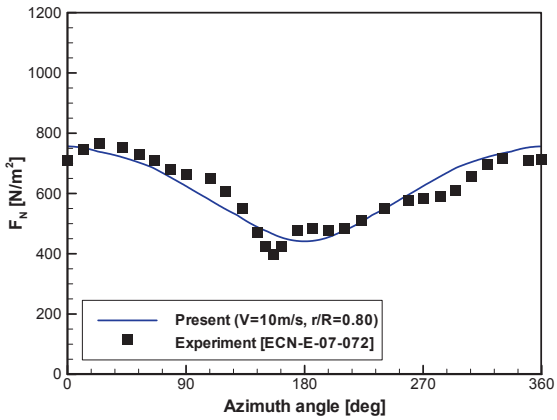

(c) r/R = 0.80

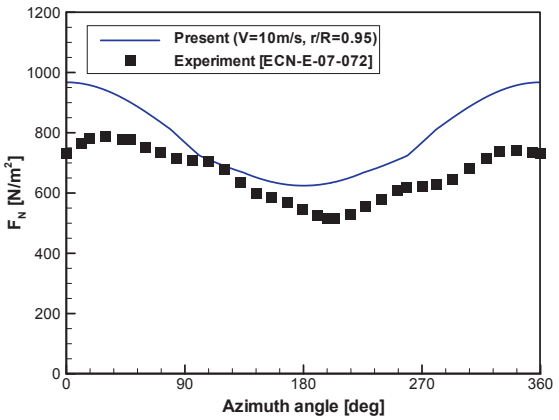

(d) r/R = 0.95

Fig. 7. Normal force distribution for wind speed of 10 m/s

azimuth angle of 180° where the blade is fully retreating *i.e.* the 12 o'clock position. We assumed that the slightly greater difference between the measured and predicted result at r/R = 0.95 compared with the other radial positions originated from the selected tip loss model. Henceforth, a comparative review for the tip loss model in addition to Prandtl's model will be necessary for a detailed investigation of the difference value at the tip position.

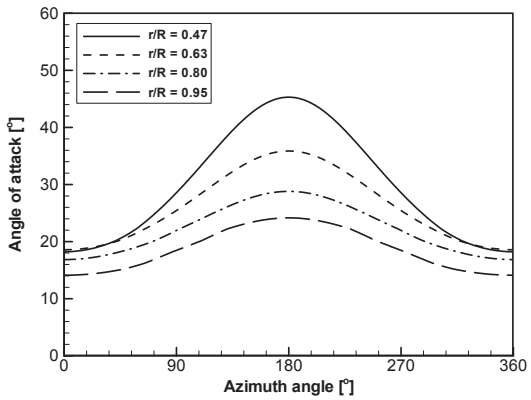

Fig. 8. Variation of angle of attack (V = 15 m/s, yaw angle = 30°)

Figure 8 shows the variation of the angles of attack with respect to the azimuth angle at the 4 radial positions of r/R = 0.47, 0.63, 0.80, and 0.95 for a wind speed of 15 m/s. From the comparison of angle of attack in Figs. 5 and 8, we can determine that the angles of attack are relatively increased due to the increased wind speed from 10 m/s to 15 m/s. The result reveals that most of the angles of attack are in the range of 15° to 45°. Therefore, most of the angles of attack exceed the stall angle of the S809 airfoil which can be estimated from Fig. 4.

The predicted normal forces at 4 radial positions for a wind speed of 15 m/s are compared with corresponding measured data as shown in Fig. 9. The oscillating trend of the normal force according to the azimuth angle is similar to that shown in Fig. 7, but the difference in value between the predicted and measured data is larger than those in Fig.

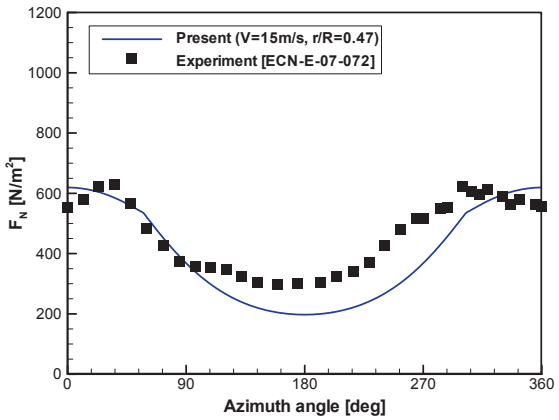

(a) r/R = 0.47

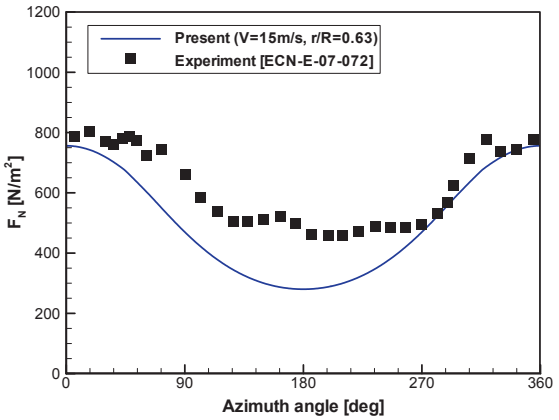

(b) r/R = 0.63

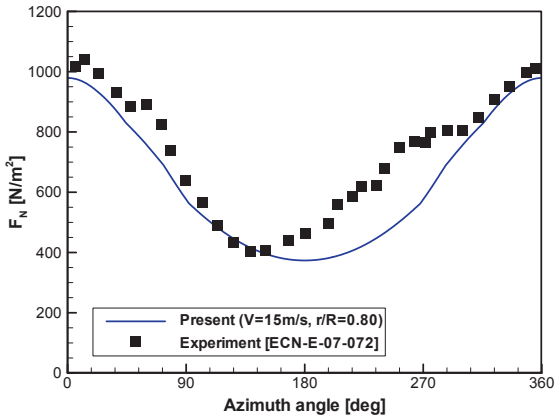

(c) r/R = 0.80

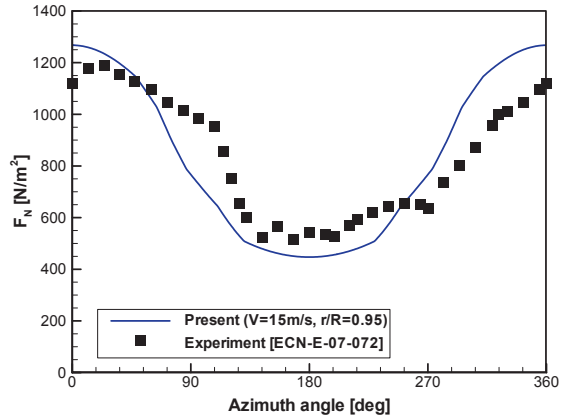

(d) r/R = 0.95

Fig. 9. Normal force distribution for wind speed of 15 m/s

DOI: http://dx.doi.org/10.5139/IJASS.2016.17.2.157

7. We believe that the extrapolated aerodynamic data using Viterna-Corrigan's method [12] for the angle of attack in the post stall range (over 24º shown in Fig. 4) would have a greater source of error. Thus, the gap is derived from the use of not-experimented extrapolated aerodynamic data rather than from the weak point of the blade element momentum theorem with simplified aerodynamic assumptions. It should be also noted that the variation in normal force may be disturbed by periodic blade deflection from the unbalance of the bending moment due to the yaw error. In spite of the gap, the accuracy of the predicted aerodynamic data is acceptable, with wind tunnel results posing similar overall value. Therefore the predicted data is able to provide sufficient values for structural or dynamic analysis for a wind turbine system.

The results of the present method are compared with those of the PHATAS [19] which is developed by the ECN for the aero-elastic analysis of a wind turbine system relying on the blade element momentum theorem. It also contains 2-D assumptions and engineering models to compute the yaw effects of the wind turbine rotor. The present method gives an in-phase signal compared with the experimental data, while the PHATAS' results have a 67º phase delay for $V = 10$ m/s and $r/R = 0.47$ as shown in Fig. 10 and Table 2. Four characteristic values for normal pressure such as mean value, $|\max(F_N)-\min(F_N)|$, mean error compared with the experimental data, and phase error show that the present method agrees better with the experimental data than the PHATAS' results. In Table 2, the value of $|\max(F_N)-\min(F_N)|$ expresses peak to peak amplitude of the normal force oscillation.

4. Conclusions

Aerodynamic loads acting on the NREL Phase VI blade were calculated numerically using a corrected blade element momentum theorem. The existing blade element momentum theorem was modified based on well-known aerodynamic corrections such as Pitt and Peters' yaw correction, Buhl's wake correction, Prandtl's tip loss model, Du and Selig's three-dimensional stall delay model. Calculated results were verified by comparing with other experimental works of 30º yaw and two given wind speeds obtained from the NASA-Ames subsonic wind tunnel. A successive under-relaxation technique was developed and applied to prevent possible failure during the iteration process.

The developed code provided results with stable convergence and fast calculation, despite the possible

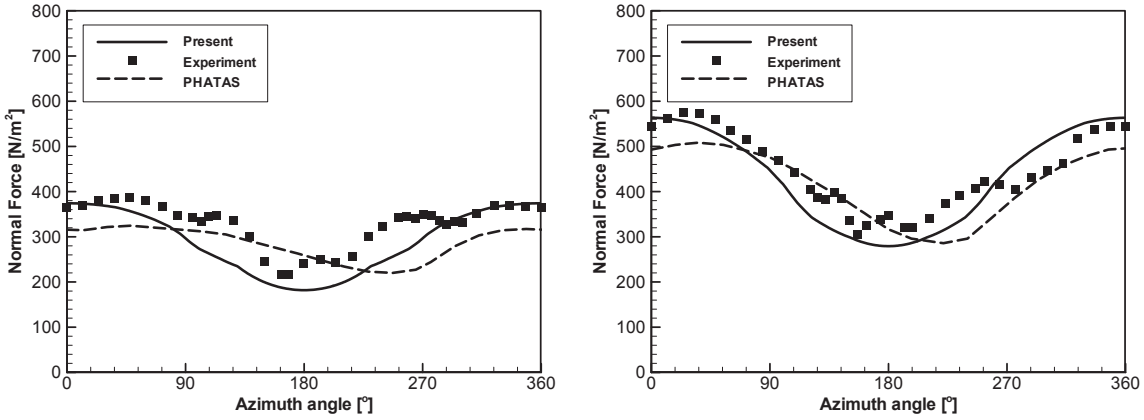

(a) $r/R = 0.47$ (b) $r/R = 0.63$

Fig. 10. Comparison with PHATAS' results ($V = 10$ m/s, yaw angle = 30°)

Table 2. Characteristic values of normal force of different methods for $V = 10$ m/s, $r/R = 0.47$

	Experiment	Present	PHATAS
Mean value	328.5	289.1	285.8
$\lvert\max(F_N)-\min(F_N)\rvert$	168.6	192.3	104.4
Mean error with experiment	-	40.4	55.1
Phase error	-	0º	67º *

* Phase error is obtained from the minimum peak value

disruptions of the classical blade element momentum theorem with a number of additional corrections applied. A yaw error yields periodic oscillation of the normal force according to the azimuth angle. The periodic change of the relative incoming wind speed on the blade element creates periodic change of the angle of attack on the blade element. Comparison between calculated and experimental results proves that the modified numerical procedure is effective in producing results with acceptably minute margins of error. The code will be useful for achieving a comprehensive tool for wind turbine design and analysis in future works

Acknowledgements

This work was supported by the New & Renewable Energy of the Korea Institute of Energy Technology Evaluation and Planning (KETEP) grant funded by the Korea government Ministry of Trade, Industry and Energy. (No. 20143010024330, SUCCESS project). This research was also supported by the "Research Base Construction Fund Support Program" funded by Chonbuk National University in 2015.

References

[1] GWEC, *Global wind report 2014*, Global Wind Energy Council, March, 2015.

[2] Kwag, D., Ryu, M., Kwon, O. and Bang, S., "Design and Installation of Meteorological Towers with Tripod Suction Piles for Offshore Wind Farms", *The 24th International Ocean and Polar Engineering Conference*, 15-20 June, Busan, Korea, 2014.

[3] IEC-61400-1, Wind Turbine Generator Systems, Part 1: Safety Requirements. International Electrotechnical Commission, Geneva, Swiss, 2005.

[4] Jonkman, J. M. and Buhl Jr, M. L., *FAST User's Guide*, NREL/EL-500-29798, NREL, March, 2004.

[5] Glauert, H., "Aerodynamic Theory", Vol. IV, Division L, Airplane propeller, chapter XI, edited by Durand W. F., Dover Publication Inc., 1963.

[6] Wilson, R. E., Lissaman, P. B. S. and Walker, S. M., "Aerodynamic Performance of Wind Turbines", Research Report ERDA/NSF/04014-76, Oregon State University, 1976, pp. 1–126.

[7] Ryu, K. W., "Optimal Aerodynamic Design and Performance Analysis for Pitch-controlled HAWT", *Journal of the Korean Society for Aeronautical and Space Sciences*, Vol. 35, No. 10, 2007, pp. 891–898.

[8] Lindenburg, C., "Investigation into Rotor Blade Aerodynamics: Analysis of the Stationary Measurements on the UAE Phase-VI Rotor in the NASA-Ames Wind Tunnel", ECN-C-03-025, ECN Wind Energy, 2003.

[9] Schepers, J. G., "Final Report of IEA Annex XX: Comparison Between Calculations and Measurements on a Wind Turbine in Yaw in the NASA-Ames Wind Tunnel", ECN-E-07-072, ECN Wind Energy, 2007.

[10] Himmelskamp, H., *Profile Investigations on a Rotating Airscrew*, Ph.D. Thesis, Gottingen University. Germany, 1945.

[11] Du, Z. and Selig, M. S., "A 3-D Stall Delay Model for Horizontal Axis Wind Turbine Performance Prediction", Proc. *1998 ASME Wind Energy Symposium, 36th AIAA Aerospace Science Meeting*, AIAA 1998-0021, 1998.

[12] Viterna, L. A. and Corrigan, R. D., "Fixed Pitch Rotor Performance of Large Horizontal Axis Wind Turbines", *Proceedings, Workshop on Large Horizontal Axis Wind Turbine*, NASA, P-2203, DOE Publication. CONF-810752, Cleveland, OH: NASA Lewis Research Center, 1981, pp. 69-85.

[13] Buhl Jr, M. L., "A New Empirical Relationship Between Thrust Coefficient and Induction Factor for the Turbulent State", Technical Report NREL/TP-500-36834, 2005.

[14] Manwell, J. F., McGowan, J. G. and Rogers, A. L., *Wind Energy Explained: Theory, Design and Applications*, John Wiley and Sons, New York, 2002.

[15] Moriarty, P. J. and Hansen, A. C., "AeroDyn Theory Manual", NREL/TP-500-36881, 2005

[16] Glauert, H., "A Classical Theory of the Autogyro", R&M No. 1111, British A. R. C., 1926.

[17] Pitt, D. M. and Peters, D. A., "Theoretical Prediction of Dynamic-inflow Derivatives", *Vertica*, Vol. 5, No. 1, 1981, pp. 21-34.

[18] Burton, T., Sharpe, D., Jenkins, N. and Bossanyi, E., *Wind Energy Handbook*, Wiley and Sons, New York, 2001.

[19] Schepers, J. G., "Final Report of IEA Annex XX: Comparison Between Calculations and Measurements on a Wind Turbine in Yaw in the NASA-Ames Wind Tunnel", ECN-E-07-072, 2007.

[20] Ramsay, R. R., Hoffmann, M. J. and Gregorek, G. M., "Effects of Grit Roughness and Pitch Ocillations on the S809 Airfoil", Revised (12/99), NREL/TP-442-7817, 1995.